



# Natural convection of hybrid nanofluids inside a partitioned porous cavity for application in solar power plants

Rasul Mohebbi<sup>1</sup> · S. A. M. Mehryan<sup>2</sup> · Mohsen Izadi<sup>3</sup> · Omid Mahian<sup>4,5</sup>

Received: 23 August 2018 / Accepted: 8 January 2019 / Published online: 22 February 2019  
© Akadémiai Kiadó, Budapest, Hungary 2019

## Abstract

The present article deals with the CFD simulation of natural convection heat transfer of a hybrid nanofluid in an inverted T-shaped cavity partitioned and saturated by two different types of porous media. Suspensions of organic and inorganic nanoparticles, i.e., MWCNTs and  $\text{Fe}_3\text{O}_4$ , in water were selected as the working fluid. The macroscopic conservation equations for the flow field and heat transfer were modeled via volume averaging the microscopic equations inside porous media over a representative elementary volume. The effects of many parameters were investigated. The parameters included the Rayleigh number ( $Ra=103\text{--}106$ ), porosity coefficient ratio of two porous media ( $\varepsilon_r=0.5\text{--}1.8$ ), volume fraction of the dispersed nanoparticles ( $\varphi=0\text{--}0.003$ ), Richardson number ( $Ri=0.1\text{--}20$ ), Darcy number ratio of two porous media ( $Dar=0.01, 1, 100$ ) and thermal conductivity ratio of two porous media ( $k_r=0.2, 0.4, 1, 5$ ). The results showed that, with an increase in the Rayleigh number, porosity ratio and Darcy number ratio and decrease in the thermal conductivity ratio, the averaged Nusselt number increased.

---

✉ Rasul Mohebbi  
Rasul\_mohebbi@du.ac.ir

✉ Mohsen Izadi  
Izadi.m@lu.ac.ir

<sup>1</sup> School of Engineering, Damghan University, P.  
O. Box 3671641167, Damghan, Iran

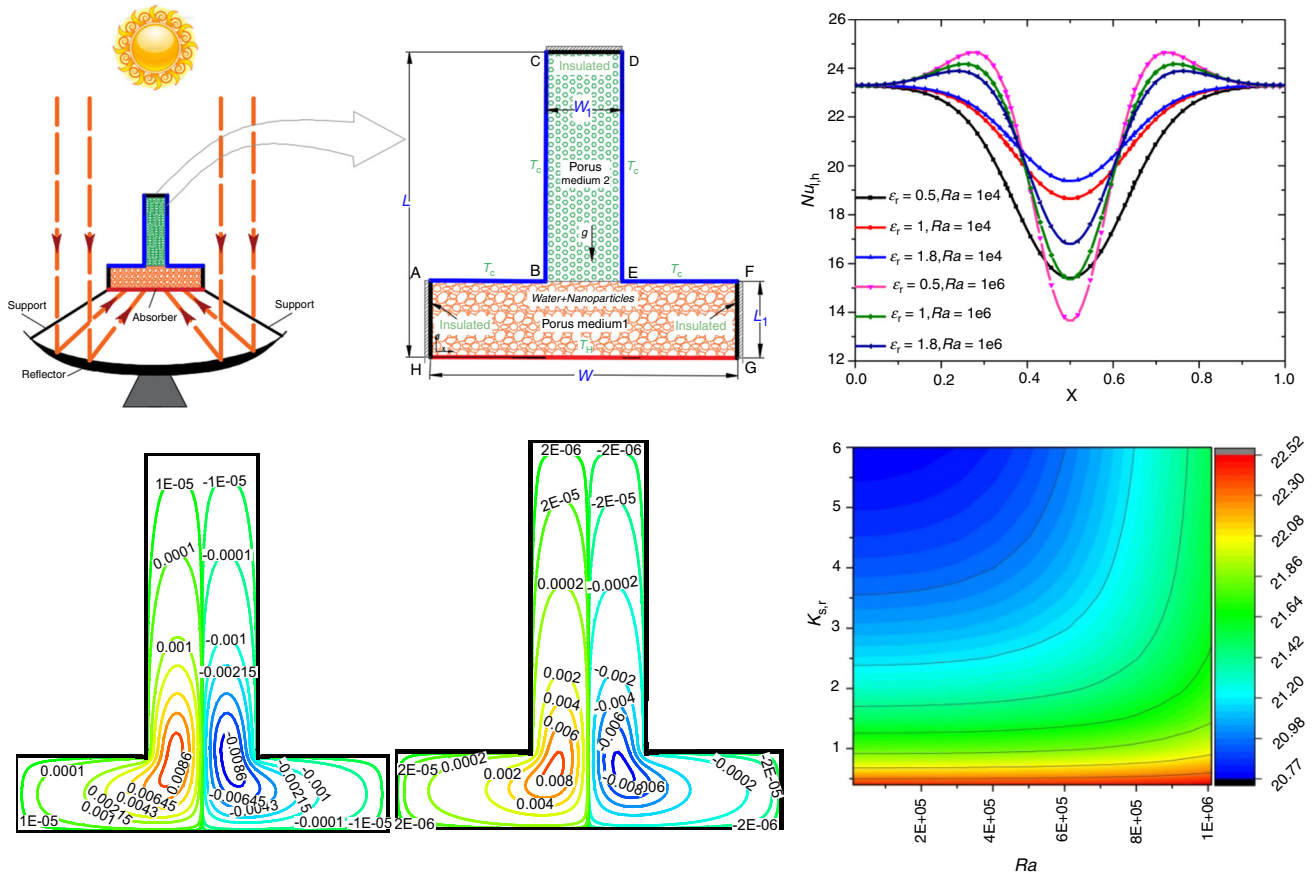
<sup>2</sup> Young Researchers and Elite Club, Yasooj Branch, Islamic  
Azad University, Yasooj, Iran

<sup>3</sup> Mechanical Engineering Department, Faculty of Engineering,  
Lorestan University, Khorramabad, Iran

<sup>4</sup> School of Chemical Engineering and Technology, Xi'an  
Jiaotong University, Xi'an 710049, Shaanxi, China

<sup>5</sup> Center for Advanced Technologies, Ferdowsi University of  
Mashhad, Mashhad, Iran

Graphical abstract



**Keywords** MWCNT–Fe<sub>3</sub>O<sub>4</sub>/water hybrid nanofluid · Natural convection · Two-layer porous medium · Inverted T-shaped enclosure

**List of symbols**

- AR Cavity obstruction ratio
- Da Darcy number
- k Thermal conductivity
- L Height of cavity
- L<sub>1</sub> Width of cavity
- Nu Nusselt number
- p Pressure
- Pr Prandtl number
- T Temperature
- u, v Nondimensional velocity components
- W Length of cavity
- W<sub>1</sub> Width of cavity
- x, y Coordinate

**Greeks symbols**

- $\varepsilon$  Porosity
- $\alpha$  Thermal diffusivity
- $\varphi$  Volume fraction
- $\beta$  Thermal expansion coefficient
- $\mu$  Dynamic viscosity
- $\rho$  Viscosity

**Subscripts**

- c Cold
- f Fluid
- h Hot
- nf Nanofluid

## Superscript

\* Dimensional parameters

## Introduction

The idea of adding solid particles to conventional liquids can be traced to the eighteenth century and became more practical with the emergence of nanotechnology. Nanofluid, a term introduced by Choi in 1995 [1], is used for mixtures of nanoscale (in the range of 1–100 nm) solid particles including metals (Cu, Fe, Al and Ag) and metal oxides (CuO, TiO<sub>2</sub>, Al<sub>2</sub>O<sub>3</sub> and SiO<sub>2</sub>), nonmetals (carbon nanotubes and graphite), and carbides (SiC) and nitrides (AlN, SiN) in a base fluid. Such fluids have appreciably greater thermal conductivity compared with common liquids, being especially used in engineering systems for cooling electronic devices, and might be able to satisfy the rising demands for an efficient rate of heat transfer.

In the last decade, researchers have paid special attention to finding optimal solutions to reduce energy consumption, which would consequently help reduce global warming. Using both porous media and nanofluids in thermal systems such as solar power plants, active nuclear waste disposal systems and so on would be a practical approach to ameliorating the thermal efficiency of such systems through heat transfer enhancement. Heat transfer enhancement is mainly created by thermal conductivity advancement of working fluid [2, 3] and the consequent decrease in boundary layer thickness as well as increase in the heat transfer contact surface, which is provided by the porous media [4]. Using nanofluid could enhance natural [5–12] and forced convection [13–18].

Over the past several years, many studies have been done on nanofluids and natural convection inside cavities fully or partially filled with porous media [12, 19–27]. In preliminary studies, Beckerman et al. [28] used the Brinkman-Forchheimer extended Darcy model to simulate the effects of the porous region on natural convection inside a vertical cavity. The researchers found that the porous layer would greatly affect the patterns of natural convection in the cavity by changing the value of the Darcy number. Baytas et al. [29] examined the problem of conduction and convection heat transfer in a porous cavity. Their findings indicated that the strength of the flow inside the cavity was thoroughly related to the ratio of solid and fluid thermal conductivity. Considering the effects of Brownian diffusion and thermophoresis, Nield and Kuznetsov [30] conducted an analytical study on the phenomenon of natural convection in a porous domain saturated by nanofluids. Chamkha and Ismael [31] examined the nanofluid natural convection in a porous cavity for different  $Ra$  numbers.

It was found that nanofluid enhanced the heat transfer rate. Also, at low Rayleigh number values, a significant increase in heat transfer inside the porous cavity with concentration was detected. Bourantas et al. [32] conducted a study on natural convection heat transfer inside a porous cavity. The cavity was equipped with a heat source on the bottom wall of the cavity and filled with a nanofluid. They found that nanofluid can increase the heat transfer rate.

Hajipour and Dehkordi [33] carried out a numerical study on nanofluid mixed convection flow in a vertical rectangular cavity that was in part packed with porous metal foam. The researchers found that, with a 0.3% nanoparticle concentration dispersed in the base fluid, a 20% increase in heat transfer could be achieved.

Nguyen et al. [34] examined natural convection heat transfer of nanofluids inside a porous cavity under variable heatings. Their results showed that the value of the Rayleigh number and nanoparticle volume fraction influenced the process of heat transfer. The heat transfer of TiO<sub>2</sub>/water nanofluid in a cavity composed of a vertical porous layer was simulated by Al-Zamily [35]. The results showed that when the heat source was placed on the bottom half of the left wall, a higher rate of heat transfer could be obtained. The results also demonstrated that the average  $Nu$  decreases as the value of the Darcy number or the thickness of the porous layer increases. Sheikholeslami and Shamlooei [36] simulated the convective flow of nanofluids inside a lid-driven cavity saturated with porous media. The researchers found that the heat transfer process improved as the Darcy and Reynolds number values increased, while the process deteriorated as the Hartmann number value increased. Sheikholeslami [37] reported impacts of the electro-hydrodynamics on coupled radiative-natural convective heat transfer of a nanofluid in a porous cavity numerically and found that  $Nu$  enhances with the permeability of porous media. Recently, Hoghoughi et al. [23] used Buongiorno's model to examine natural convection of a nanofluid inside a porous wavy wall cavity. Effects of some passive parameters have been extensively considered using a local thermal nonequilibrium model. The researchers reported that  $Nu$  declines as heat inside the enclosure increases.

Based on the authors' best knowledge, no work on the investigation of natural convection of nanofluid flow in a partitioned porous cavity has been reported so far. Therefore, the present study aims to fill this gap by studying the natural convection of a hybrid nanofluid (MWCNT-Fe<sub>3</sub>O<sub>4</sub>/water) inside an inverted T-shaped cavity filled with two different porous media. The effect of the Rayleigh number, nanoparticle volume fraction, porosity coefficient ratio, Darcy number ratio and thermal conductivity ratio of two porous media on the hydrodynamic and thermal

characteristics was investigated. The results of this study can be applied to the design of solar power plants or thermal storage systems.

### Mathematics of the problem

The geometry of the problem is shown in Fig. 1. The geometry is an inverted T-shaped enclosure by height  $L^*$ , length  $W^*$  ( $L^* = W^*$ ), width  $W_1^*$  and  $L_1^*$  and cavity aspect ratio  $L_1^*/L^* = 0.2$  filled by a hybrid nanofluid. Two discrete porous media fill the cavity by different properties so that they affect the thermal and flow field of the hybrid nanofluid. It is assumed that nanofluid is homogeneous, there is no sedimentation in porous media, and the size of nanoparticles is much bigger than that of the porous holes. The macroscopic equations of an incompressible flow in a porous medium were calculated by volume averaging the microscopic conservation equations using the REV [38]:

$$\frac{\partial u^*}{\partial x^*} + \frac{\partial v^*}{\partial y^*} = 0 \tag{1}$$

$$\begin{aligned} \frac{\rho_{nf}}{\varepsilon_i^2} \left( u^* \frac{\partial u^*}{\partial x^*} + v^* \frac{\partial u^*}{\partial y^*} \right) = & -\frac{\partial p^*}{\partial x^*} + \frac{\mu_{nf}}{\varepsilon_i} \left( \frac{\partial^2 u^*}{\partial x^{*2}} + \frac{\partial^2 u^*}{\partial y^{*2}} \right) \\ & - \frac{\mu_{nf}}{K_i} u^* - \frac{1.75}{\sqrt{150}} \frac{\rho_{nf}}{\sqrt{K_i}} \frac{\sqrt{u^{*2} + v^{*2}}}{\varepsilon_i^{3/2}} u^* \end{aligned} \tag{2}$$

$$\begin{aligned} \frac{\rho_{nf}}{\varepsilon_i^2} \left( u^* \frac{\partial v^*}{\partial x^*} + v^* \frac{\partial v^*}{\partial y^*} \right) = & -\frac{\partial p^*}{\partial y^*} + \frac{\mu_{nf}}{\varepsilon_i} \left( \frac{\partial^2 v^*}{\partial x^{*2}} + \frac{\partial^2 v^*}{\partial y^{*2}} \right) - \frac{\mu_{nf}}{K_i} v^* \\ & - \frac{1.75}{\sqrt{150}} \frac{\rho_{nf}}{\sqrt{K_i}} \frac{\sqrt{u^{*2} + v^{*2}}}{\varepsilon_i^{3/2}} v^* + \rho_{nf} g \beta_{nf} (T_{nf}^* - T_c^*) \end{aligned} \tag{3}$$

$$(\rho c_p)_{nf} \left( u^* \frac{\partial T_{nf}^*}{\partial x^*} + v^* \frac{\partial T_{nf}^*}{\partial y^*} \right) = k_{nf,m_i} \left( \frac{\partial^2 T_{nf}^*}{\partial x^{*2}} + \frac{\partial^2 T_{nf}^*}{\partial y^{*2}} \right) \tag{4}$$

$$k_{nf,m_i} = \varepsilon_i k_{nf} + (1 - \varepsilon_i) k_{s,i} \tag{5}$$

The star superscript signifies the dimensional variables. Also, the  $i$  index shows the properties of the two porous layers defined by subscripts 1 and 2.

The boundary conditions in the dimensional  $x^*$  and  $y^*$  coordinates are

$$\text{At } AB, BC, DE, EF \quad T^* = T_c^* \quad u^* = v^* = 0 \tag{6}$$

$$\text{At } HG \quad T^* = T_h^* \quad u^* = v^* = 0 \tag{7}$$

$$\text{At } CD, AH, FG \quad \frac{\partial T^*}{\partial y^*} = 0 \tag{8}$$

At the interface of the two different porous layers, the continuity of mass and heat flux was held on their interface.

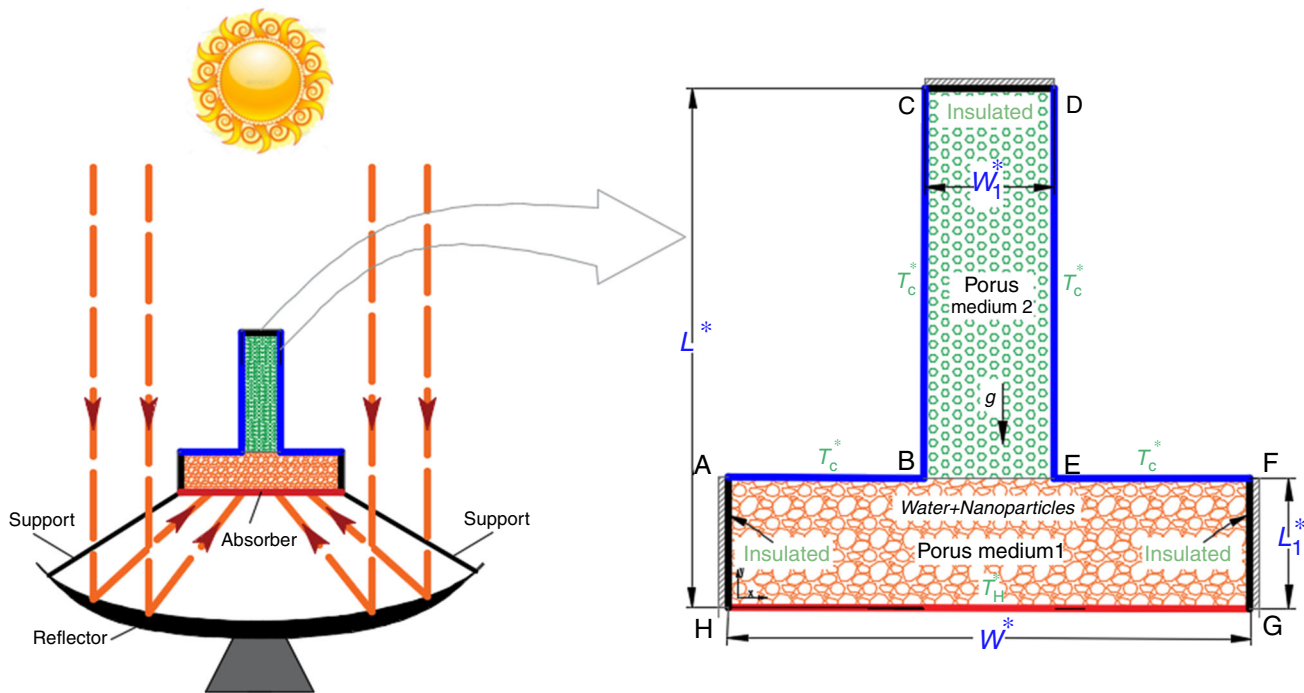


Fig. 1 Schematic of the problem

**Table 1** The thermophysical properties of carbon nanotube–Fe<sub>3</sub>O<sub>4</sub> hybrid nanofluid for different volume fractions and temperatures [39]

Volume fraction/%	<i>T</i> /°C	$\rho$ /kg m <sup>-3</sup>	<i>k</i> /W m <sup>-1</sup> K <sup>-1</sup>	$\mu$ /mp s	<i>c<sub>p</sub></i> /J kg K	<i>Pr</i>
$\varphi=0.0$ (host fluid)	20	998.5	0.602	0.79	4182	5.5
	40	992.0	0.631	0.54	4179	3.61
$\varphi=0.1$	20	1002.34	0.6734	0.91	4182.66	5.64
	40	995.85	0.72	0.61	4179.66	3.56
$\varphi=0.3$	20	1010.04	0.6856	1.01	4183.99	6.10
	40	1003.56	0.7656	0.76	4180.99	4.14

$$\begin{aligned}
 u_{\text{porous1}}^* &= u_{\text{porous2}}^*, & v_{\text{porous1}}^* &= v_{\text{porous2}}^* \\
 \mu_{\text{nf,eff}} \frac{\partial u^*}{\partial n^*} \Big|_{\text{porous1}} &= \mu_{\text{nf,eff}} \frac{\partial u^*}{\partial n^*} \Big|_{\text{porous2}}, & \mu_{\text{nf,eff}} \frac{\partial v^*}{\partial n^*} \Big|_{\text{porous1}} &= \mu_{\text{nf,eff}} \frac{\partial v^*}{\partial n^*} \Big|_{\text{porous2}} \\
 &= \mu_{\text{nf,eff}} \frac{\partial v^*}{\partial n^*} \Big|_{\text{porous2}}, & T_{\text{nf}}^* \Big|_{\text{porous1}} &= T_{\text{nf}}^* \Big|_{\text{porous2}} \\
 k_{\text{nf,m}} \frac{\partial T_{\text{nf}}^*}{\partial n^*} \Big|_{\text{porous1}} &= k_{\text{nf,m}} \frac{\partial T_{\text{nf}}^*}{\partial n^*} \Big|_{\text{porous2}}
 \end{aligned} \tag{9}$$

where  $k_{\text{nf,m}} = \varepsilon k_{\text{nf}} + (1 - \varepsilon)k_s$ ,  $\mu_{\text{nf,eff}} = \frac{\mu_{\text{nf}}}{\varepsilon}$ .

To analyze the parametric dimensionless, the following parameters were employed to obtain the dimensionless forms for the equations modeled above:

$$\begin{aligned}
 x &= x^*/L^*, & y &= y^*/L^*, & n &= n^*/L^*, \\
 T_{\text{nf}} &= \frac{(T_{\text{nf}}^* - T_c^*)}{(T_h^* - T_c^*)}, & u &= \frac{u^*}{\alpha_{\text{bf}}/L^*}, \\
 v &= \frac{v^*}{\alpha_{\text{bf}}/L^*} & \text{and} & p &= \frac{p^*}{\rho_{\text{bf}}(\alpha_{\text{bf}}/L^*)^2}
 \end{aligned} \tag{10}$$

Hence, we have the following:

$$\frac{\partial u}{\partial x} + \frac{\partial v}{\partial y} = 0 \tag{11}$$

$$\begin{aligned}
 \frac{1}{\varepsilon_i^2} \left( u \frac{\partial u}{\partial x} + v \frac{\partial u}{\partial y} \right) &= -\rho_r \frac{\partial p}{\partial x} + \frac{Pr}{\varepsilon_i} \mu_r \rho_r \left( \frac{\partial^2 u}{\partial x^2} + \frac{\partial^2 u}{\partial y^2} \right) \\
 - \frac{Pr}{Da_i} \mu_r \rho_r u - \frac{1.75}{\sqrt{150}} \frac{\sqrt{u^2 + v^2}}{\sqrt{Da_i} \cdot \varepsilon_i} u
 \end{aligned} \tag{12}$$

$$\begin{aligned}
 \frac{1}{\varepsilon_i^2} \left( u \frac{\partial v}{\partial x} + v \frac{\partial v}{\partial y} \right) &= -\rho_r \frac{\partial p}{\partial y} + \frac{Pr}{\varepsilon_i} \mu_r \rho_r \left( \frac{\partial^2 v}{\partial x^2} + \frac{\partial^2 v}{\partial y^2} \right) \\
 - \frac{Pr}{Da_i} \mu_r \rho_r v - \frac{1.75}{\sqrt{150}} \frac{\sqrt{u^2 + v^2}}{\sqrt{Da_i} \cdot \varepsilon_E} v + RaPr\beta_r T_{\text{nf}}
 \end{aligned} \tag{13}$$

$$u \frac{\partial T_{\text{nf}}}{\partial x} + v \frac{\partial T_{\text{nf}}}{\partial y} = \alpha_r \left( \frac{\partial^2 T_{\text{nf}}}{\partial x^2} + \frac{\partial^2 T_{\text{nf}}}{\partial y^2} \right) \tag{14}$$

$$\alpha_r = \frac{\alpha_{\text{nf,m}}}{\alpha_{\text{bf}}}, \quad \alpha_{\text{nf,m}} = \frac{k_{\text{nf,m}}}{(\rho c_p)_{\text{nf}}} \tag{15}$$

*Ra*, *Pr* and *Da* of the above equations, respectively, are

$$Ra = \frac{g \rho_{\text{bf}} \beta_{\text{bf}} (T_h^* - T_c^*) L^3}{\alpha_{\text{bf}} \nu_{\text{bf}}}, \quad Da_i = \frac{K_i}{L^{*2}}, \quad Pr = \frac{\nu_{\text{bf}}}{\alpha_{\text{bf}}} \tag{16}$$

The boundary conditions subjected to the bounds are:

$$\begin{aligned}
 u_{\text{porous1}} &= u_{\text{porous2}}, & v_{\text{porous1}} &= v_{\text{porous2}} \\
 \frac{1}{\varepsilon} \frac{\partial u}{\partial n} \Big|_{\text{porous1}} &= \frac{1}{\varepsilon} \frac{\partial u}{\partial n} \Big|_{\text{porous2}}, & \frac{\partial v}{\partial n} \Big|_{\text{porous1}} &= \frac{1}{\varepsilon} \frac{\partial v}{\partial n} \Big|_{\text{porous2}} \\
 T_{\text{nf}} \Big|_{\text{porous1}} &= T_{\text{nf}} \Big|_{\text{porous2}} \\
 \frac{\partial T_{\text{nf}}}{\partial n} \Big|_{\text{porous1}} &= \left( \frac{k_{\text{nf,m}_2}}{k_{\text{nf,m}_1}} \right) \frac{\partial T_{\text{nf}}}{\partial n} \Big|_{\text{porous2}}
 \end{aligned} \tag{17}$$

The rate of local heat transfer over the hot wall is calculated through the following equation:

$$Nu_x = - \frac{k_{\text{nf,m}}}{k_{\text{bf}}} \left( \frac{\partial T}{\partial y} \right)_{x=0} \tag{18}$$

The integration of the above equations gives the total heat transfer rate:

$$Nu_{\text{avg}} = \int_0^1 Nu_x \, dx \tag{19}$$

### Thermophysical properties of the nanofluid

A review of hybrid nanofluids showed that there is no established relation for calculating the thermophysical properties of these new types of suspensions. Hence, the current study employs the experimental data of MWCNT–Fe<sub>3</sub>O<sub>4</sub> hybrid nanofluid for calculating properties as depicted in Table 1. In addition, Table 2 illustrates the thermophysical properties of Fe<sub>3</sub>O<sub>4</sub> and the MWCNT nanoparticles. Other thermophysical properties of the hybrid nanofluid can be calculated using the relations given below:

$$\rho_{\text{nf}} = (1 - \varphi)\rho_{\text{bf}} + \varphi\rho_{\text{np}} \tag{20}$$

$$\rho_{\text{nf}} \beta_{\text{nf}} = (1 - \varphi)(\rho\beta)_{\text{bf}} + \varphi(\rho\beta)_{\text{np}} \tag{21}$$

**Table 2** Thermophysical properties of Fe<sub>3</sub>O<sub>4</sub> and MWCNT [8]

Property	$\rho/\text{kg m}^{-3}$	$c_p/\text{J kg}^{-1} \text{K}^{-1}$	$k/w \text{ m}^{-1} \text{K}^{-1}$	$\beta/\text{K}^{-1}$
Fe <sub>3</sub> O <sub>4</sub>	5810	670	6	$1.3 \times 10^{-5}$
MWCNT	2100	711	3000	$4.2 \times 10^{-5}$

**Table 3** Grid study:  $Ra=1e4$ ,  $\varepsilon_r=1$ ,  $\varepsilon_1=0.5$ ,  $k_{s,1}=5$ ,  $k_{s,r}=1$ ,  $Da_1=1e-2$ ,  $Da_r=1$ ,  $\phi_{hnf}=0.3\%$

Grid number	3600	5075	6400	8775	11500
$Nu_{avg}$	21.794	21.793	21.792	21.791	21.791

**Table 4** Average Nusselt number in a porous triangular-shaped enclosure occupied by Cu–water nanofluid

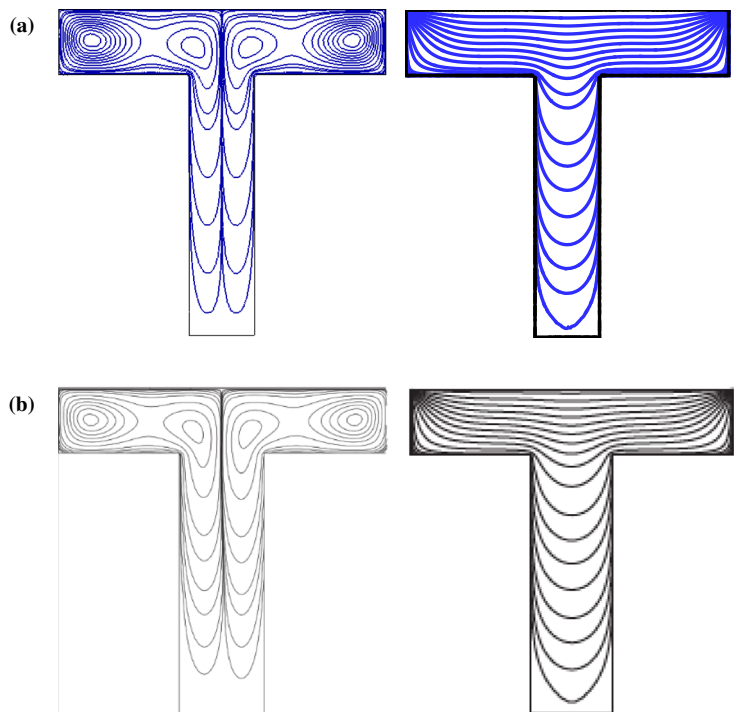
$Ra$	$\phi$	Sun and Pop [40]	Sheremet et al. [41]	Present work
500	0	9.66	9.65	9.64
1000	0.1	9.42	9.41	9.42
500	0	13.9	14.05	13.96
1000	0.2	12.85	12.84	12.85

$$\beta_{np} = \frac{\beta_{MWCNT} w_{MWCNT} + \beta_{Fe_3O_4} w_{Fe_3O_4}}{w_{MWCNT} + w_{Fe_3O_4}} \quad (22)$$

$$\alpha_{nf} = \frac{k_{nf}}{(\rho C_p)_{nf}} \quad (23)$$

where  $\phi$  represents the value of volume fraction for dispersed nanoparticles.

**Fig. 2** Streamlines and isotherm lines of **a** the current study and **b** Esfe et al. [42] (reprinted with permission from Elsevier)



### Grid independency and code validation

Grid independency study is performed using several different grids. The study shows that the mesh size of 8775 is optimal (see Table 3). The accuracy of the numerical procedure was checked and validated against the available results in the literature. As shown in Table 4, Figs. 2 and 3, the present numerical procedure is in good agreement with the published results.

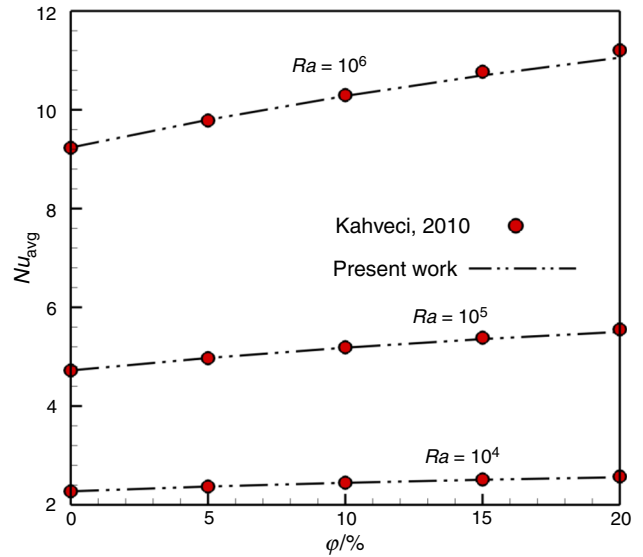


**Fig. 3** Variation of  $Nu_{avg}$  according to the volume fraction of nanoparticles for the different values of  $Ra$  resulting from Kahveci [43] and the present study



### Results and discussion

The present study deals with the free convective heat transfer of a MWCNT–Fe<sub>3</sub>O<sub>4</sub>/water hybrid nanofluid within a contrariwise T-shaped cavity saturated by two different porous medium. The results are presented for various Rayleigh number values, the porosity ratio of porous media ( $\epsilon_r = \epsilon_1/\epsilon_2$ ), nanoparticle volume fraction, Richardson number, Darcy number ratio ( $Da_r = Da_1/Da_2$ ) and thermal conductivity ratio of the solid phases of two porous media ( $k_{s,r} = k_{s,1}/k_{s,2}$ ).

The effect of the presence of nanoparticles on streamlines for low and high values of the Rayleigh number ( $Ra$ ) in the porous medium at different porosity ratios is illustrated in Fig. 4 for  $\epsilon_1 = 0.5$ ,  $k_{s,1} = 5$ ,  $k_{s,r} = 1$ ,  $Da_1 = 1e-2$ ,  $Da_r = 1$  and  $\phi_{hnf} = 0.3\%$ . As seen, in a fixed porosity ratio, two symmetrical convective cells (clockwise circulation in the right and counterclockwise circulation in the left) are shaped inside the cavity at low Rayleigh number values. This is caused by the buoyancy forces effected by the difference in fluid temperature and motivates the fluid to ascend in the middle and come down on the sides of the cavity. Increasing the  $Ra$  leads to the increment of the

**Fig. 4** Variation of streamlines with the porosity coefficient of two porous media and Rayleigh number at  $\epsilon_1 = 0.5$ ,  $k_{s,1} = 5$ ,  $k_{s,r} = 1$ ,  $Da_1 = 1e-2$ ,  $Da_r = 1$ ,  $\phi_{hnf} = 0.3\%$

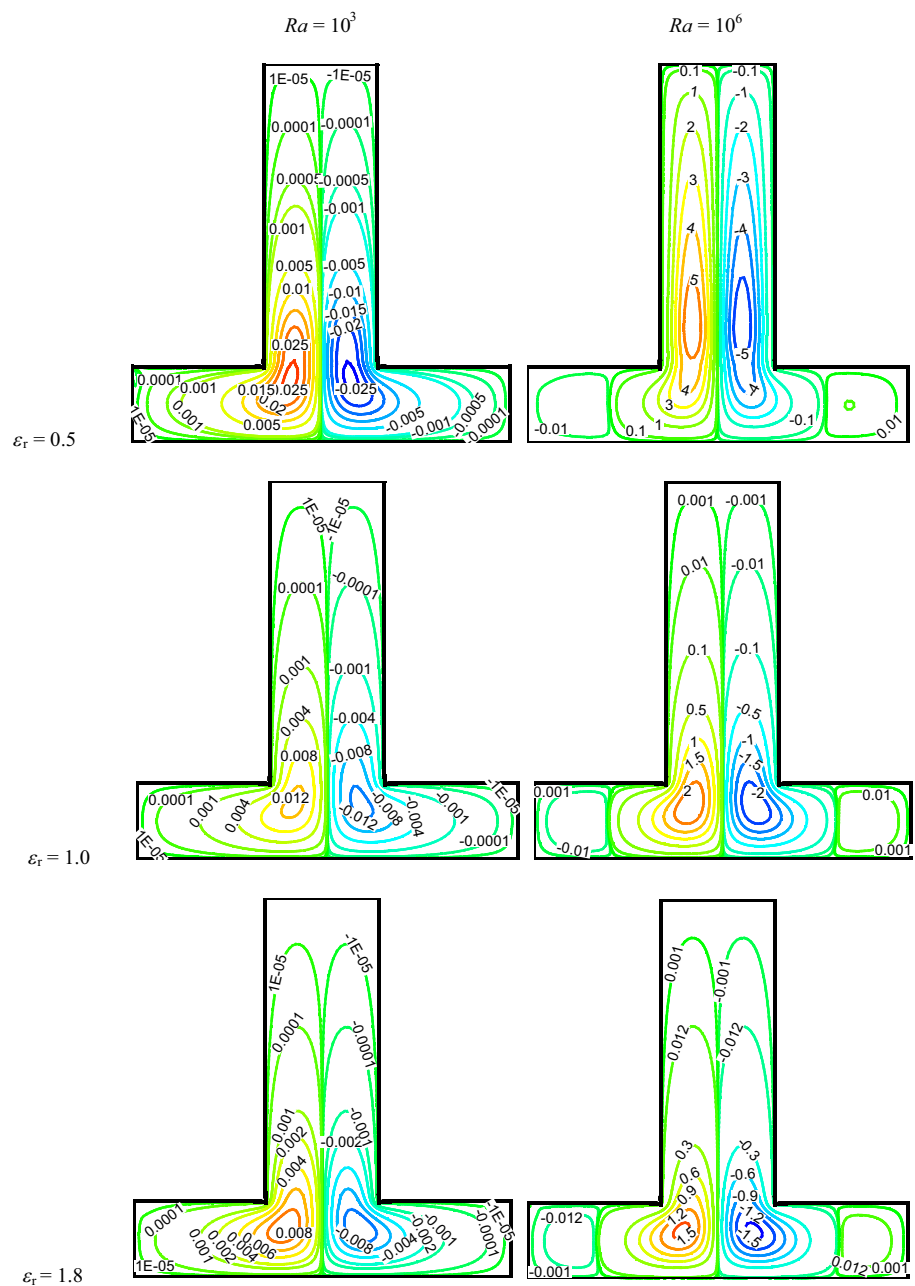
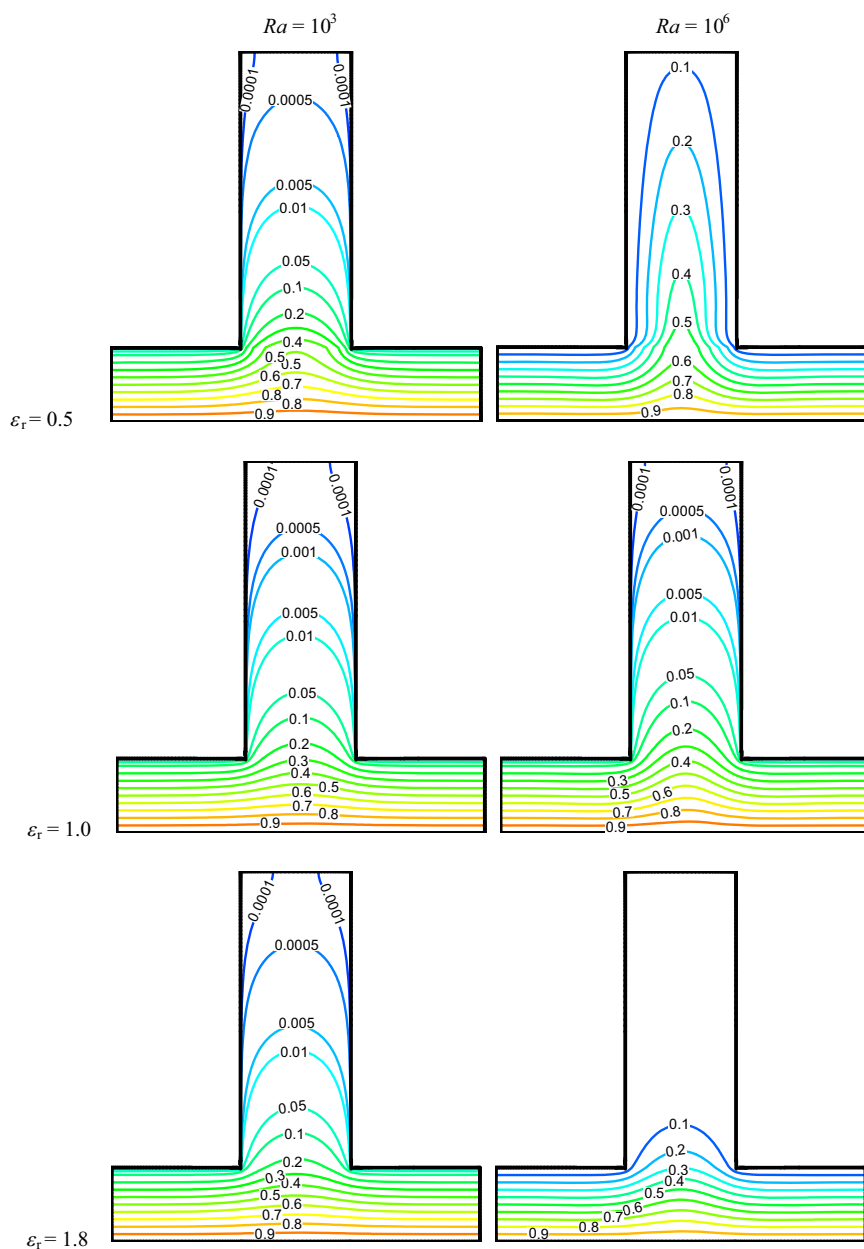


**Fig. 5** Variation of isotherm lines with the porosity coefficient of two porous media and Rayleigh number at  $\varepsilon_1=0.5$ ,  $k_{s,1}=5$ ,  $k_{s,r}=1$ ,  $Da_1=1e-2$ ,  $Da_r=1$ ,  $\varphi_{hnf}=0.3\%$



buoyancy force, which increases the strength of the main vortices and occupies the whole of enclosure. The formation of two secondary recirculation zones in the vicinity of the side walls is due to domination of the convection heat transfer. Also, at a fixed  $Ra$  number, when the  $\varepsilon_r$  parameter increases, the power of the circulation over the porous layers is decreased.

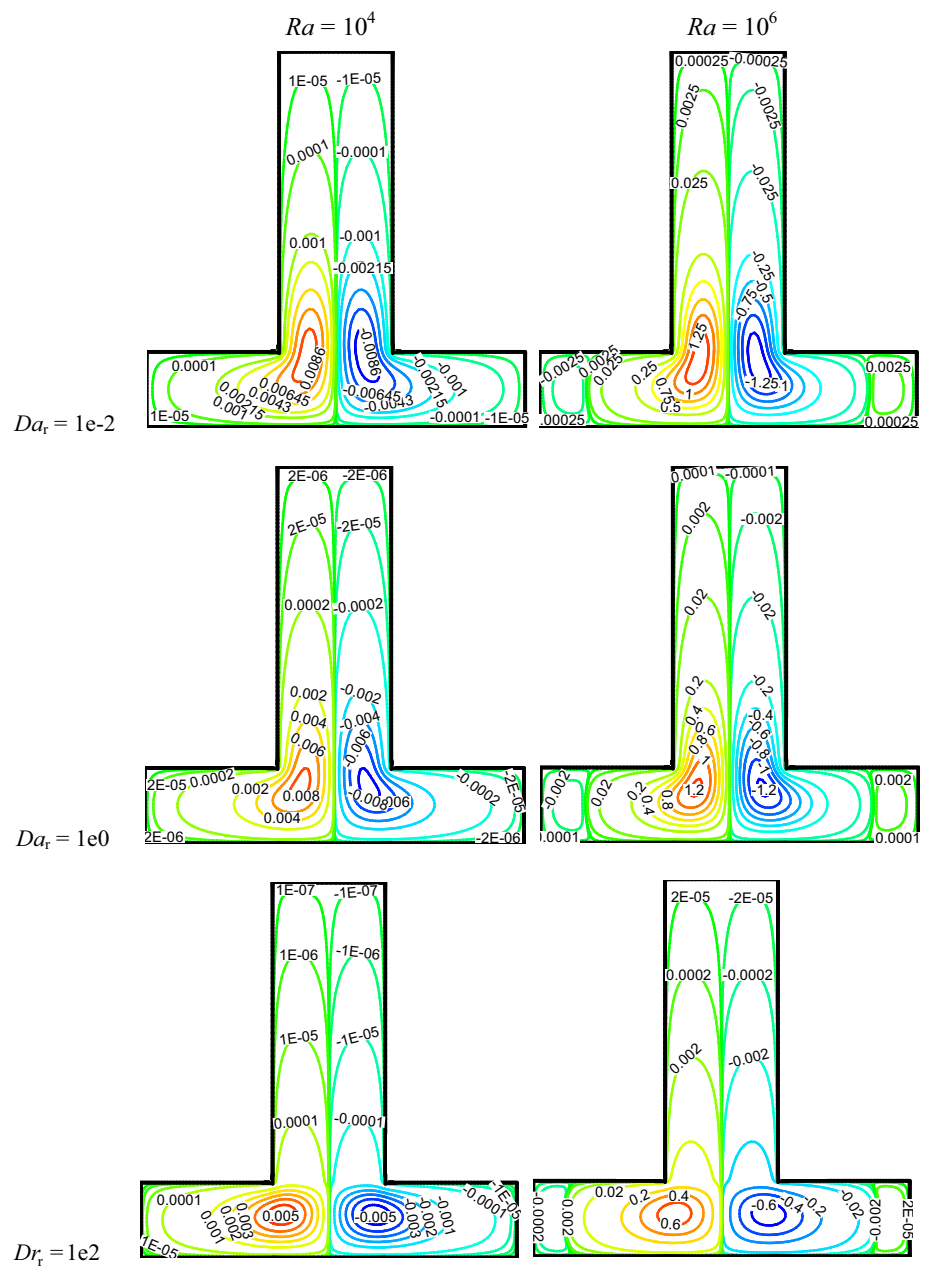
Figure 5 presents the isotherm lines for the nanofluid at different values of the Rayleigh number and porosity coefficient for  $\varepsilon_1=0.5$ ,  $k_{s,1}=5$ ,  $k_{s,r}=1$ ,  $Da_1=1e-2$ ,  $Da_r=1$  and  $\varphi_{hnf}=0.3\%$ . Symmetrical temperature patterns are

observed inside the enclosure. Although isotherm lines would not significantly change for different porosity ratio values, an intensive change in the shape of isotherm lines occurred at  $Ra=10^6$  for an increment in the porosity ratio.

The bottom porous layer is heated from below. Interaction of the hot-temperature wave from porous layer 1 and cold-temperature wave from the cold besides the walls occurred inside porous layer 2. As expected, the penetration of the hot regime throughout the upper porous media increases by decreasing the porosity ratio, so that this rate is noticeable in high  $Ra$  numbers. Moreover, for the higher



**Fig. 6** Variation of streamlines with the Darcy number ratio of two porous media and Rayleigh number at  $\epsilon_1=0.5$ ,  $\epsilon_r=1$ ,  $k_{s,1}=5$ ,  $k_{s,r}=1$ ,  $Da_1=1e-3$ ,  $\phi_{hnf}=0.3\%$



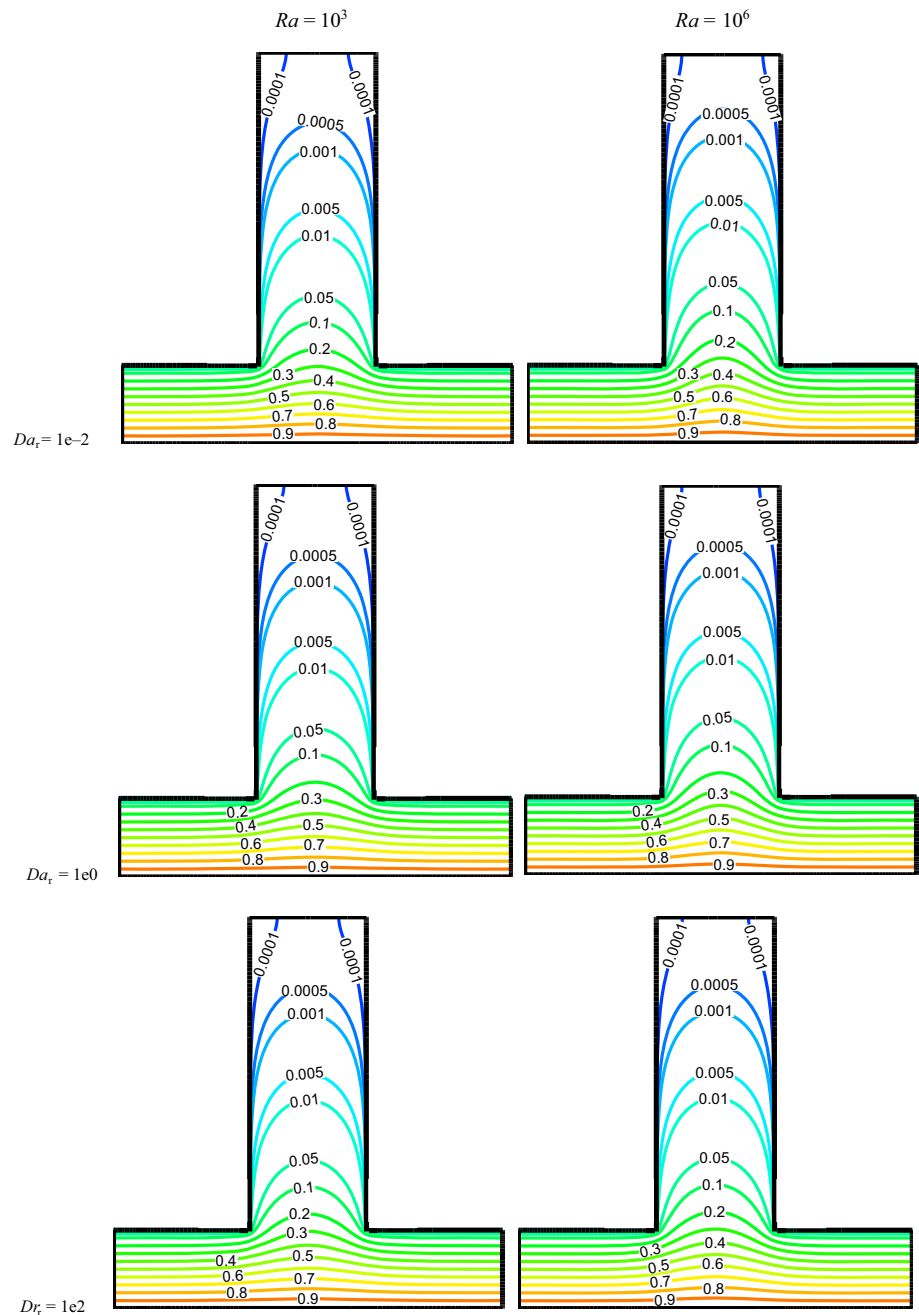
values of the  $Ra$  number, the layers of the thermal boundary close to the bottom walls become thinner.

The effects of the Darcy number ratio of two porous media and the Rayleigh number at  $\epsilon_1=0.5$ ,  $\epsilon_r=1$ ,  $k_{s,1}=5$ ,  $k_{s,r}=1$ ,  $Da_1=1e-3$  and  $\phi_{hnf}=0.3\%$  on streamlines and isotherm lines are shown in Figs. 6 and 7. As shown in Fig. 6, a decrease in  $Da_r$  is related to the extension observed in the permeability of the layer on the bottom porous medium through the upper porous medium by increasing the vortex strength. This moves the center of the main elliptical shape vortices from the bottom part of the cavity toward the center of the enclosure. Also, two weak secondary vortices are generated apart from the main vortices at  $Ra=10^6$ . The

vortices with the lowest strength would, respectively, occur on the top and bottom sides in the centerline of the cavity. An overview of the isotherm lines is shown in Fig. 7, which reveals that there is no significant difference between the patterns of the temperature field when the parameters  $Da_r$  and  $Ra$  increase. In addition, while the temperature gradient in the neighborhood of the cold vertical boundary in the upper porous medium is low, the gradient is high in the vicinity of the hot horizontal wall in the lower porous medium.

Figures 8 and 9 show the effects of the thermal conductivity ratio of two porous media and the Rayleigh number at  $\epsilon_1=0.5$ ,  $\epsilon_r=1$ ,  $k_{s,1}=5$ ,  $Da_1=10^{-2}$ ,  $Da_r=1$ ,  $\phi_{hnf}=$

**Fig. 7** Variation of isotherm lines with the Darcy number ratio of two porous media and Rayleigh number at  $\varepsilon_1=0.5$ ,  $\varepsilon_r=1$ ,  $k_{s,1}=5$ ,  $k_{s,r}=1$ ,  $Da_1=1e-3$ ,  $\phi_{hnf}=0.3\%$



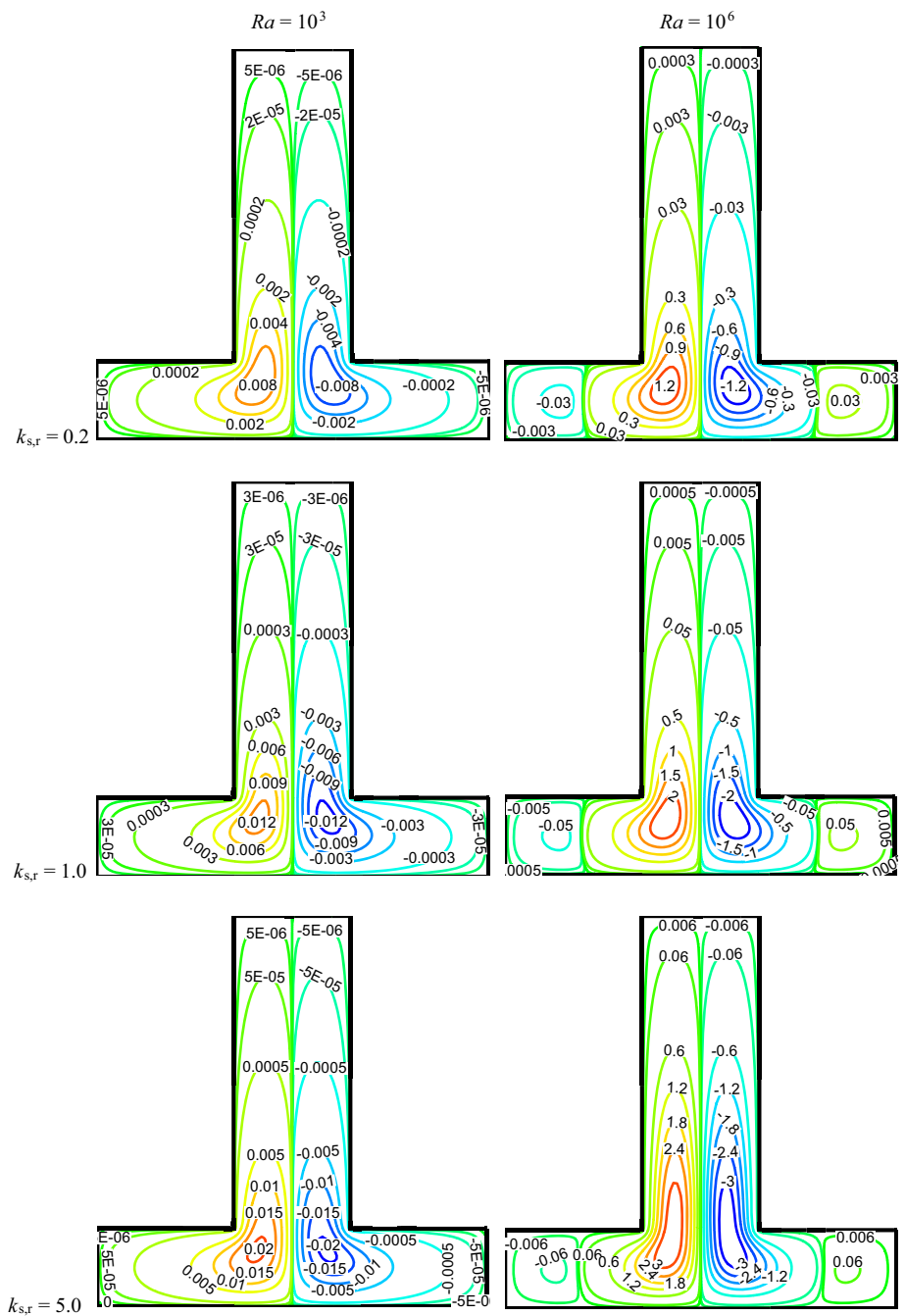
0.3% on streamlines and isotherm lines, respectively. An increase in the thermal conductivity ratio creates longer and stronger vortices in the cavity (see Fig. 8) and pushes the hot plume fluid to the upper section of the cavity (see Fig. 9) at a constant  $Ra$  number. This phenomenon leads to the increase in heat exchange between the two porous media. At  $k_{s,r}=5$  and  $Ra=10^6$ , a large penetration of flow within porous layer 2 occurs, and the strong circulation leads to dancer streamlines. It is obvious that the isotherm lines are more concentrated in the lower than upper part of

the cavity, which leads to a strong temperature gradient in these regions.

The graphs illustrated in Fig. 10a, b show the variation trend in the values of the local Nusselt number over the bottom hot wall in the  $x$ -direction and average  $Nu$  number-based  $Ra$  and  $\varepsilon_r$ .

The other parameters are selected equally as  $k_{s,1}=5$ ,  $Da_1=1e-2$ ,  $Da_r=1$  and  $\phi_{hnf}=0.3\%$ . The drastic reduction in the local Nusselt number at the center of the cavity is observed for  $Ra=10^4$ . The thick thermal boundary layer in this region has the highest thermal resistance against heat

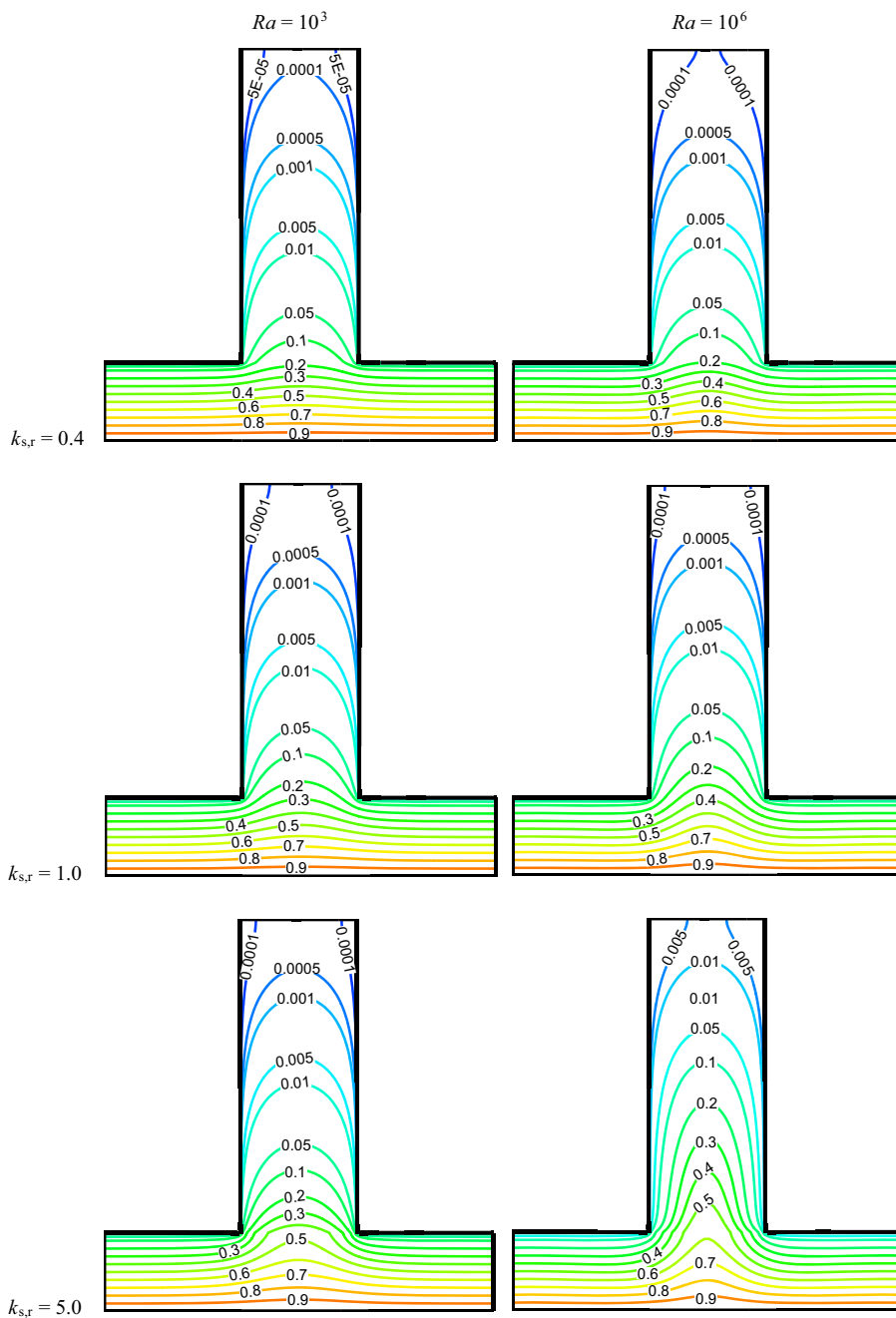
**Fig. 8** Variation of streamlines with the thermal conductivity ratio of two porous media and Rayleigh number at  $\varepsilon_1=0.5$ ,  $\varepsilon_r=1$ ,  $k_{s,1}=5$ ,  $Da_1=1e-2$ ,  $Da_r=1$ ,  $\phi_{hnf}=0.3\%$



transfer, so the minimum heat transfer rate occurs locally at the center part of the hot wall. Also, the vortices remove the heat from the hot boundary at the center of the enclosure and transmits it to the cold walls (see Figs. 4 and 5) so the rate of the local  $Nu$  number has the minimum value at  $x=0$  for the mentioned  $Ra$  number. Furthermore, the reduction in local  $Nu$  number along the cavity length becomes less at higher porosity ratio values (as shown in Fig. 5).

Different trends occur for  $Ra=10^6$  at fixed  $\varepsilon_r$ ; this implies that the heat transfer rate increases along the  $x$ -direction and reaches a maximum value at  $x=0.3$  (similar position on the right side of the cavity, i.e.,  $x=0.7$ ). The reason for the increase in heat transfer could be easily deduced from the formation of secondary flow and its movement toward the main vortex in the opposite direction so that the thermal boundary layer becomes thinner. In the mentioned position,  $\varepsilon_r=0.5$  shows the maximum heat transfer rate. Anyway, from  $x=0.3$  to  $0.5$ , a sharp reduction

**Fig. 9** Variation of isotherm lines with the thermal conductivity ratio of two porous media and Rayleigh number at  $\epsilon_1=0.5$ ,  $\epsilon_r=1$ ,  $k_{s,1}=5$ ,  $Da_1=1e-2$ ,  $Da_r=1$ ,  $\phi_{hnf}=0.3\%$



in the local  $Nu$  number occurs in the enclosure, especially at low  $\epsilon_r$  values, because of better circulation of fluid flow in the upper part of the cavity and production of less crowded isotherm contours because of the thicker thermal boundary layer on the lower wall of the cavity.

According to Fig. 10b, with increasing  $Ra$  number at a constant  $\epsilon_r$ , the magnitude of the buoyant force increases, which causes an increase in flow strength and in turn a heat transfer increment. At higher  $\epsilon_r$ ,  $Nu$  slightly increases by an

increment of  $Ra$ . At a low porosity ratio value, the fluid flow is strong because of low flow resistance, which can be boosted at a high  $Ra$  number. This improves the ventilation and makes a bigger difference for  $Nu_{avg}$  from  $10^3$  to  $10^6$ .

The local variation of the Nusselt number on the hot wall and surface variation of  $Nu_{avg}$  with  $Ra$  and  $Da_r$  are shown in Fig. 11a and b, respectively. Figure 11a shows that the enhancement of the local  $Nu$  number at a fixed  $Da_r$  starts from the beginning at  $Ra=10^6$  and increases with a

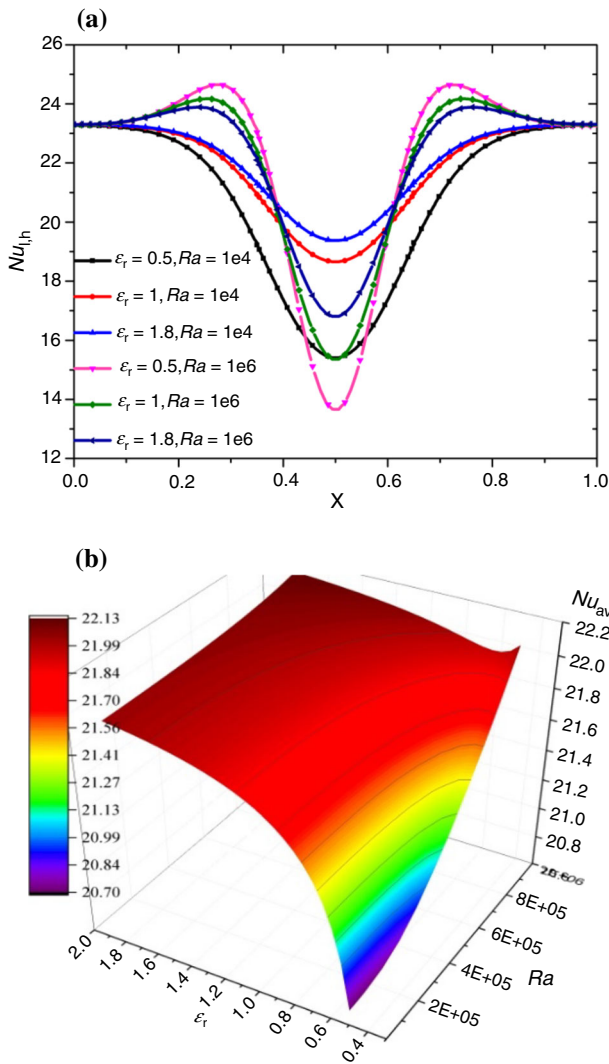


**Fig. 10** a Local variation of the Nusselt number on the hot wall and b surface variation of  $Nu_{avg}$  with  $Ra$  and  $\epsilon_r$  at  $\phi_{hnf}=0.3\%$

mild slope until  $x=0.3$  (because of the confrontation of two vortices with each other, as seen in Fig. 6). After that, this rising trend reduces precipitously until the middle section of the enclosure, and after this value the mentioned trends repeat reversely. By increasing the  $Da_r$  in low  $Ra$  numbers, there is no difference in the rate of heat transfer. According to Fig. 11b, at a high  $Ra$  number, the heat transfer increases with an increasing  $Da_r$  parameter. With increasing  $Da_r$ , the rate of fluid flow through porous region 2 decreases (see Fig. 6); therefore, the temperature in porous medium 1 increases and the convection heat transfer increases. At low  $Ra$  values, the value of  $Nu_{avg}$  does not change significantly with  $Da_r$ .

Finally, Fig. 12 [cases (a) and (b)] shows the impact of the thermal conductivity ratio in the porous medium on the local and average  $Nu$  number at different  $Ra$  numbers. As

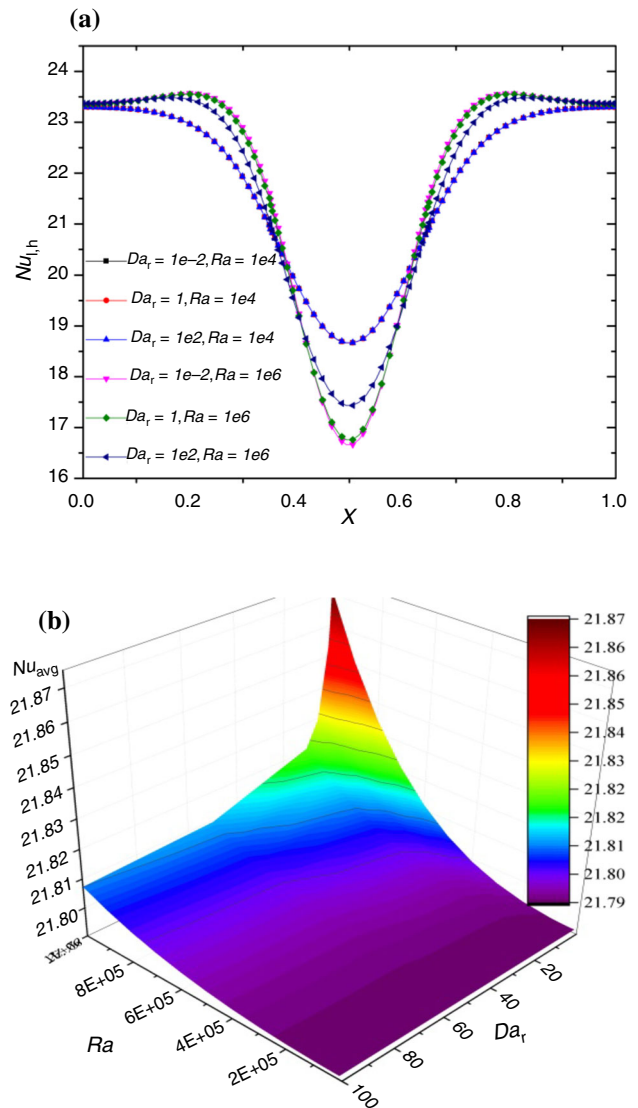


**Fig. 11** a Local variation of the Nusselt number on the hot wall and b surface variation of  $Nu_{avg}$  with  $Ra$  and  $Da_r$

shown in Fig. 12a, when  $k_{s,r}$  increases, the local  $Nu$  number decreases totally, but at  $Ra=10^6$ , the heat transfer rate increases slowly until the point approaching the main vortices in the cavity, which leads to a temperature rise near the wall. Also, according to Fig. 12b, at a fixed  $Ra$  number, as the thermal conductivity ratio of porous media increases, an obvious decrease in the value of the average Nusselt number is observed. The reduction rates are equal to 7.36% and 3.049% at  $Ra=10^3$  and  $10^6$ , respectively. Such behavior points to the fact that an increase in the value of the  $k_{s,r}$  leads to a rise in the thermal conductivity ratio for porous medium 1 compared with that of porous medium 2.

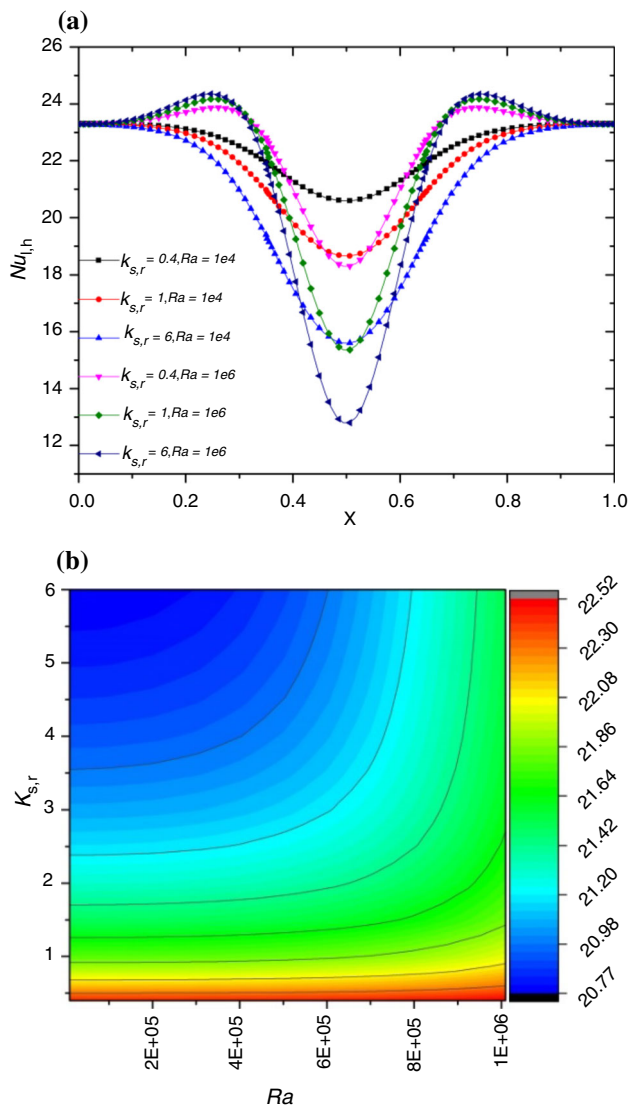


**Fig. 12** a Local variation of the Nusselt number on the hot wall and b surface variation of  $Nu_{avg}$  with  $Ra$  and  $k_{s,r}$

## Conclusions

The natural convective flow and heat transfer of MWCNT–Fe<sub>3</sub>O<sub>4</sub>/water hybrid nanofluid in a partitioned cavity consisting of multilayer porous media were studied numerically. The effects of different parameters such as the  $Ra$ , porosity coefficient ratio, Darcy number ratio and thermal conductivity ratio on streamlines, isotherm lines and the local and averaged  $Nu$  number were investigated. The main findings are listed:

- At a given  $Ra$  number, by the increment of  $\varepsilon_r$ , the circulation power inside the porous layers decreases.
- The penetration of the hot regime throughout the upper porous media increases by decreasing the porosity ratio.

- An increase in the thermal conductivity ratio creates longer and stronger vortices in the cavity (see Fig. 7) and pushes the hot plume fluid to the upper section of the cavity (see Fig. 8) at a constant  $Ra$  number.
- $Nu_{ave}$  at  $Ra=10^6$  is 6.23 times larger than  $Nu_{ave}$  at  $Ra=10^3$  for  $\varepsilon_r=0.5$ , while  $Nu_{ave}$  at  $Ra=10^6$  is 0.63 times larger than  $Nu_{ave}$  at  $Ra=10^3$  for  $\varepsilon_r=1.8$ .
- At a fixed  $Ra$  number, when the thermal conductivity ratio of the porous media goes up, an obvious decrease in the average Nusselt number is observed.

## References

1. Chol SU, Estman JA. Enhancing thermal conductivity of fluids with nanoparticles. ASME Publ Fed. 1995;231:99–106.
2. Mohebbi R, Izadi M, Delouei AA, Sajjadi H. Effect of MWCNT–Fe<sub>3</sub>O<sub>4</sub>/water hybrid nanofluid on the thermal performance of ribbed channel with apart sections of heating and cooling. J Thermal Anal Calorim. 2018. <https://doi.org/10.1007/s10973-018-7483-5>.
3. Matori A, Mohebbi R, Hashemi Z, Ma Y. Lattice Boltzmann study of multi-walled carbon nanotube (MWCNT)–Fe<sub>3</sub>O<sub>4</sub>/water hybrid nanofluids natural convection heat transfer in a  $\Pi$ -shaped cavity equipped by hot obstacle. J Thermal Anal Calorim. 2018. <https://doi.org/10.1007/s10973-018-7881-8>.
4. Nazari M, Kayhani MH, Mohebbi R. Heat transfer enhancement in a channel partially filled with a porous block: lattice Boltzmann method. Int J Mod Phys C. 2013;24:1350060.
5. Abchouyeh MA, Mohebbi R, Fard OS. Lattice Boltzmann simulation of nanofluid natural convection heat transfer in a channel with a sinusoidal obstacle. Int J Mod Phys C. 2018;29:1850079.
6. Ma Y, Mohebbi R, Rashidi MM, Manca O, Yang Z. Numerical investigation of MHD effects on nanofluid heat transfer in a baffled U-shaped enclosure using lattice Boltzmann method. J Thermal Anal Calorim. 2018. <https://doi.org/10.1007/s10973-018-7518-y>.
7. Ma Y, Mohebbi R, Rashidi MM, Yang Z, Sheremet MA. Numerical study of MHD nanofluid natural convection in a baffled U-shaped enclosure. Int J Heat Mass Transf. 2019;130:123–34.
8. Ma Y, Mohebbi R, Rashidi MM, Yang Z. MHD forced convection of MWCNT–Fe<sub>3</sub>O<sub>4</sub>/water hybrid nanofluid in a partially heated  $\tau$ -shaped channel using LBM. J Thermal Anal Calorim. 2018. <https://doi.org/10.1007/s10973-018-7788-4>.
9. Izadi M, Mohebbi R, Chamkha A, Pop I. Effects of cavity and heat source aspect ratios on natural convection of a nanofluid in a C-shaped cavity using lattice Boltzmann method. Int J Numer Methods Heat Fluid Flow. 2018;28:1930–55.
10. Mohebbi R, Izadi M, Chamkha AJ. Heat source location and natural convection in a C-shaped enclosure saturated by a nanofluid. Phys Fluids. 2017;29:122009.
11. Ranjbar P, Mohebbi R, Heidari H. Numerical investigation of nanofluids heat transfer in a channel consists of rectangular cavities by lattice Boltzmann method. Int J Modern Phys C. 2018;29(11):1850108.
12. Izadi M, Hoghoughi G, Mohebbi R, Sheremet M. Nanoparticle migration and natural convection heat transfer of Cu–water nanofluid inside a porous undulant-wall enclosure using LTNE and two-phase model. J Mol Liq. 2018;261:357–72.



13. Mohebbi R, Lakzayi H, Sidik NAC, Japar WMAA. Lattice Boltzmann method based study of the heat transfer augmentation associated with Cu/water nanofluid in a channel with surface mounted blocks. *Int J Heat Mass Transf.* 2018;117:425–35.
14. Mohebbi R, Rashidi MM, Izadi M, Sidik NAC, Xian HW. Forced convection of nanofluids in an extended surfaces channel using lattice Boltzmann method. *Int J Heat Mass Transf.* 2018;117:1291–303.
15. Izadi M, Mohebbi R, Karimi D, Sheremet MA. Numerical simulation of natural convection heat transfer inside a  $\perp$  shaped cavity filled by a MWCNT–Fe<sub>3</sub>O<sub>4</sub>/water hybrid nanofluids using LBM. *Chem Eng Process Process Intensif.* 2018;125:56–66.
16. Izadi M, Shahmardan MM, Maghrebi MJ, Behzadmehr A. Numerical study of developed laminar mixed convection of Al<sub>2</sub>O<sub>3</sub>/water nanofluid in an annulus. *Chem Eng Commun.* 2013;200:878–94.
17. Izadi M, Shahmardan MM, Behzadmehr A. Richardson number ratio effect on laminar mixed convection of a nanofluid flow in an annulus. *Int J Comput Methods Eng Sci Mech.* 2013;14:304–16.
18. Izadi M, Behzadmehr A, Shahmardan MM. Effects of inclination angle on laminar mixed convection of a nanofluid flowing through an annulus. *Chem Eng Commun.* 2015;202:1693–702.
19. Mehryan SA, Izadi M, Sheremet MA. Analysis of conjugate natural convection within a porous square enclosure occupied with micropolar nanofluid using local thermal non-equilibrium model. *J Mol Liq.* 2018;250:353–68.
20. Noghrehabadi A, Behseresht A, Ghalambaz M, Behseresht J. Natural-convection flow of nanofluids over vertical cone embedded in non-Darcy porous media. *J Thermophys Heat Transf.* 2013;27:334–41.
21. Noghrehabadi A, Behseresht A, Ghalambaz M. Natural convection of nanofluid over vertical plate embedded in porous medium: prescribed surface heat flux. *Appl Math Mech.* 2013;34:669–86.
22. Behseresht A, Noghrehabadi A, Ghalambaz M. Natural-convection heat and mass transfer from a vertical cone in porous media filled with nanofluids using the practical ranges of nanofluids thermo-physical properties. *Chem Eng Res Des.* 2014;92:447–52.
23. Hoghoughi G, Izadi M, Oztop HF, Abu-Hamdeh N. Effect of geometrical parameters on natural convection in a porous undulant-wall enclosure saturated by a nanofluid using Buongiorno's model. *J Mol Liq.* 2018;255:148–59.
24. Ghalambaz M, Behseresht A, Behseresht J, Chamkha A. Effects of nanoparticles diameter and concentration on natural convection of the Al<sub>2</sub>O<sub>3</sub>–water nanofluids considering variable thermal conductivity around a vertical cone in porous media. *Adv Powder Technol.* 2015;26:224–35.
25. Ghalambaz M, Sheremet MA, Pop I. Free convection in a parallelogrammic porous cavity filled with a nanofluid using Tiwari and Das' nanofluid model. *PLoS ONE.* 2015;10:e0126486.
26. Varol Y, Oztop HF, Pop I. Numerical analysis of natural convection for a porous rectangular enclosure with sinusoidally varying temperature profile on the bottom wall. *Int Commun Heat Mass Transf.* 2008;35:56–64.
27. Izadi M, Mohebbi R, Delouei AA, Sajjadi H. Natural convection of a Magnetizable hybrid nanofluid inside a porous enclosure subjected to two variable magnetic fields. *Int J Mech Sci.* 2019;151:154–169.
28. Beckermann C, Ramadhyani S, Viskanta R. Natural convection flow and heat transfer between a fluid layer and a porous layer inside a rectangular enclosure. *J Heat Transf.* 1987;109:363–70.
29. Baytaş AC, Liaqat A, Groşan T, Pop I. Conjugate natural convection in a square porous cavity. *Heat Mass Transf.* 2001;37:467–73.
30. Nield DA, Kuznetsov AV. The Cheng–Minkowycz problem for natural convective boundary-layer flow in a porous medium saturated by a nanofluid. *Int J Heat Mass Transf.* 2009;52:5792–5.
31. Chamkha AJ, Ismael MA. Conjugate heat transfer in a porous cavity filled with nanofluids and heated by a triangular thick wall. *Int J Thermal Sci.* 2013;67:135–51.
32. Bourantas GC, Skouras ED, Loukopoulos VC, Burganos VN. Heat transfer and natural convection of nanofluids in porous media. *Eur J Mech B/Fluids.* 2014;43:45–56.
33. Hajipour M, Dehkordi AM. Mixed-convection flow of Al<sub>2</sub>O<sub>3</sub>–H<sub>2</sub>O nanofluid in a channel partially filled with porous metal foam: experimental and numerical study. *Exp Thermal Fluid Sci.* 2014;53:49–56.
34. Nguyen MT, Aly AM, Lee S-W. Natural convection in a non-Darcy porous cavity filled with Cu–water nanofluid using the characteristic-based split procedure in finite-element method. *Numer Heat Transf Part A Appl.* 2015;67:224–47.
35. Al-Zamily AMJ. Analysis of natural convection and entropy generation in a cavity filled with multi-layers of porous medium and nanofluid with a heat generation. *Int J Heat Mass Transf.* 2017;106:1218–31.
36. Sheikholeslami M, Shamlooei M. Convective flow of nanofluid inside a lid driven porous cavity using CVFEM. *Physica B.* 2017;521:239–50.
37. Sheikholeslami M. Numerical investigation of nanofluid free convection under the influence of electric field in a porous enclosure. *J Mol Liq.* 2018;249:1212–21.
38. Nield DA, Bejan A. *Convection in porous media.* Berlin: Springer; 2006.
39. Sundar LS, Singh MK, Sousa ACM. Enhanced heat transfer and friction factor of MWCNT–Fe<sub>3</sub>O<sub>4</sub>/water hybrid nanofluids. *Int Commun Heat Mass Transf.* 2014;52:73–83.
40. Sun Q, Pop I. Free convection in a triangle cavity filled with a porous medium saturated with nanofluids with flush mounted heater on the wall. *Int J Thermal Sci.* 2011;50:2141–53.
41. Sheremet MA, Grosan T, Pop I. Free convection in a square cavity filled with a porous medium saturated by nanofluid using Tiwari and Das' nanofluid model. *Transp Porous Media.* 2015;106:595–610.
42. Esfe MH, Arani AAA, Yan W-M, Aghaei A. Natural convection in T-shaped cavities filled with water-based suspensions of COOH-functionalized multi walled carbon nanotubes. *Int J Mech Sci.* 2017;121:21–32.
43. Kahveci K. Buoyancy driven heat transfer of nanofluids in a tilted enclosure. *J Heat Transf.* 2010;132:62501.

#### Publisher's Note

Springer Nature remains neutral with regard to jurisdictional claims in published maps and institutional affiliations.